

GALAXY GROUPS IN THE SDSS DR4: II. HALO OCCUPATION STATISTICS

XIAOHU YANG^{1,4}, H.J. MO², FRANK C. VAN DEN BOSCH³*Draft version October 31, 2018*

ABSTRACT

We investigate various galaxy occupation statistics of dark matter halos using a large galaxy group catalogue constructed from the Sloan Digital Sky Survey Data Release 4 (SDSS DR4) with an adaptive halo-based group finder. The conditional luminosity function (CLF), which describes the luminosity distribution of galaxies in halos of a given mass, is measured separately for all, red and blue galaxies, as well as in terms of central and satellite galaxies. The CLFs for central and satellite galaxies can be well modelled with a log-normal distribution and a modified Schechter form, respectively. About 85% of the central galaxies and about 80% of the satellite galaxies in halos with masses $M_h \gtrsim 10^{14} h^{-1} M_\odot$ are red galaxies. These numbers decrease to 50% and 40%, respectively, in halos with $M_h \sim 10^{12} h^{-1} M_\odot$. For halos of a given mass, the distribution of the luminosities of central galaxies, L_c , has a dispersion of about 0.15 dex. The mean luminosity (stellar mass) of the central galaxies scales with halo mass as $L_c \propto M_h^{0.17}$ ($M_{*,c} \propto M_h^{0.22}$) for halos with masses $M \gg 10^{12.5} h^{-1} M_\odot$, and both relations are significantly steeper for less massive halos. We also measure the luminosity (stellar mass) gap between the first and second brightest (most massive) member galaxies, $\log L_1 - \log L_2$ ($\log M_{*,1} - \log M_{*,2}$). These gap statistics, especially in halos with $M_h \lesssim 10^{14.0} h^{-1} M_\odot$, indicate that the luminosities of central galaxies are clearly distinct from those of their satellites. The fraction of fossil groups, defined as those groups with $\log L_1 - \log L_2 \geq 0.8$, ranges from $\sim 2.5\%$ for groups with $M_h \sim 10^{14} h^{-1} M_\odot$ to 18-60% for groups with $M_h \sim 10^{13} h^{-1} M_\odot$. The number distribution of satellite galaxies in groups of a given mass follows a Poisson distribution, in agreement with the occupation statistics of dark matter sub-halos. This provides strong support for the standard lore that satellite galaxies reside in sub-halos. Finally, we measure the fraction of satellites, which changes from $\sim 5.0\%$ for galaxies with $^{0.1}M_r - 5 \log h \sim -22.0$ to $\sim 40\%$ for galaxies with $^{0.1}M_r - 5 \log h \sim -17.0$.

Subject headings: dark matter - large-scale structure of the universe - galaxies: halos - methods: statistical

1. INTRODUCTION

In recent years, the halo occupation distribution and conditional luminosity function have become powerful statistical measures to probe the link between galaxies and their hosting dark matter halos. Although these statistical measures themselves do not give physical explanations of how galaxies form and evolve, they provide important constraints on various physical processes that govern the formation and evolution of galaxies, such as gravitational instability, gas cooling, star formation, merging, tidal stripping and heating, and a variety of feedback processes. In particular, they constrain how their efficiencies scale with halo mass.

The halo occupation distribution (hereafter HOD), $P(N|M)$, which gives the probability of finding N galaxies (with some specified properties) in a halo of mass M , has been extensively used to study the galaxy distribution in dark matter halos and galaxy clustering on large scales (e.g. Jing, Mo & Börner 1998; Peacock & Smith 2000; Seljak 2000; Scoccimarro et al. 2001; Jing, Börner

& Suto 2002; Berlind & Weinberg 2002; Bullock, Wechsler & Somerville 2002; Scranton 2002; Kang et al. 2002; Marinoni & Hudson 2002; Zheng et al. 2002; Magliocchetti & Porciani 2003; Berlind et al. 2003; Zehavi et al. 2004, 2005; Zheng et al. 2005; Tinker et al. 2005). The conditional luminosity function (CLF), $\Phi(L|M)dL$, which refines the HOD statistic by considering the average number of galaxies with luminosity $L \pm dL/2$ that reside in a halo of mass M , has also been extensively investigated (Yang, Mo & van den Bosch 2003; van den Bosch, Yang & Mo 2003; Vale & Ostriker 2004, 2006; Cooray 2006; van den Bosch et al. 2007a) and has been applied to various redshift surveys, such as the 2dFGRS, the Sloan Digital Sky Survey (SDSS) and DEEP2 (e.g. Yan, Madgwick & White 2003; Yang et al. 2004; Mo et al. 2004; Wang et al. 2004; Zehavi et al. 2005; Yan, White & Coil 2004). These investigations demonstrate that the halo occupation statistics are very useful in establishing and describing the connection between galaxies and dark matter halos. Furthermore, they also indicate that the galaxy/dark halo connection can provide important constraints on cosmology (e.g., van den Bosch, Mo & Yang 2003; Zheng & Weinberg 2007). Finally, the HOD/CLF framework also allows one to split the galaxy population in centrals and satellites, and to describe their properties separately (e.g. Cooray 2005; White et al. 2007; Zheng et al. 2007).

As has been pointed out in Yang et al. (2005c; hereafter Y05c), a shortcoming of the HOD/CLF models is

¹ Shanghai Astronomical Observatory, the Partner Group of MPA, Nandan Road 80, Shanghai 200030, China; E-mail: xhyang@shao.ac.cn

² Department of Astronomy, University of Massachusetts, Amherst MA 01003-9305

³ Max-Planck-Institute for Astronomy, Königstuhl 17, D-69117 Heidelberg, Germany

⁴ Joint Institute for Galaxy and Cosmology (JOINGC) of Shanghai Astronomical Observatory and University of Science and Technology of China

that the results are not completely model independent. Typically, assumptions have to be made regarding the functional form of either $P(N|M)$ or $\Phi(L|M)$. Moreover, in all HOD/CLF studies to date, the occupation distributions have been determined in an indirect way: the free parameters of the assumed functional form are constrained using *statistical* data on the abundance and clustering properties of the galaxy population. One may hope to circumvent this shortcoming by directly measure the dark matter distribution around galaxies. Such measurements can in principle be obtained through gravitational lensing and X-ray observations. However, both methods are hampered by requirements on the data quality and uncertainties related to the interpretation of the data. For instance, weak lensing measurements, which requires high-quality imaging, typically needs to resort to the stacking of many lens galaxies in order to get a detectable signal, but this stacking severely complicates the interpretation in terms of the halo masses of the lens galaxies. In the case of X-ray observations, robust constraints can only be obtained for massive clusters, but even here the interpretation of the data can be complicated due to the presence of substructure and deviations from hydrostatic equilibrium. An alternative method to directly probe the galaxy - dark halo connection is to use galaxy groups as a representation of dark matter halos and to study how the galaxy population changes with the properties of the groups (e.g., Y05c; Zandivarez et al. 2006; Robotham et al. 2006; Hansen et al. 2007).

Recently, we have constructed a large galaxy group catalogue based on the Sloan Digital Sky Survey Data Release 4 (SDSS DR4), using an adaptive halo-based group finder (Yang et al. 2007; Paper I; Y07 hereafter). Detailed tests with mock galaxy catalogues have shown that this group finder is very successful in associating galaxies according to their common dark matter halos. In particular, the group finder performs reliably not only for rich systems, but also for poor systems, including isolated central galaxies in low mass halos. This makes it possible to study the galaxy-halo connection for systems covering a large dynamic range in masses. Various observational selection effects have been taken into account, especially the survey edge effects and fiber collisions. The halo masses for the groups are estimated according to the abundance match, using the characteristic group luminosity and stellar masses (see §2 below). According to tests with mock galaxy catalogues, the halo masses are estimated with a standard deviation of about 0.3 dex. With these well-defined galaxy group catalogues, one can not only study the properties of galaxies in different groups (e.g. Y05c; Yang et al. 2005d; Collister & Lahav 2005; van den Bosch et al. 2005; Robotham et al. 2006; Zandivarez et al. 2006; Weinmann et al. 2006a,b; van den Bosch et al. 2007b; McIntosh et al. 2007), but also probe how dark matter halos trace the large-scale structure of the Universe (e.g. Yang et al. 2005b, 2006; Coil et al. 2006; Berlind et al. 2007; Wang et al. 2007 in preparation). In this paper, which is the second in a series, we use the SDSS DR4 group catalogue to probe various occupation statistics and measure the CLFs for different populations of galaxies.

This paper is organized as follows: In Section 2 we describe the data (galaxy and group catalogues) used in this paper. Section 3 presents our measurement of

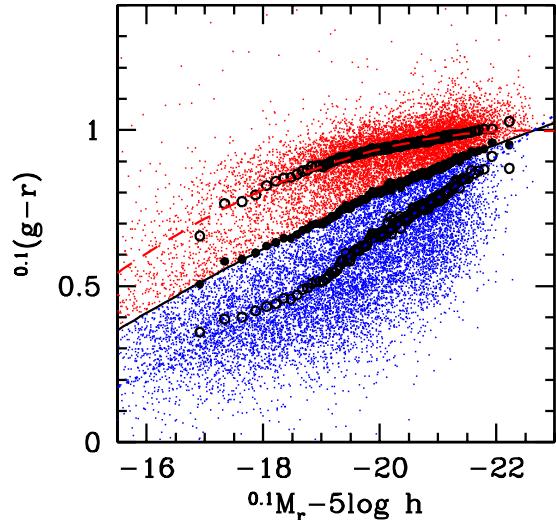


FIG. 1.— The color-magnitude relation for galaxies in our group sample. The open circles indicate the Gaussian peaks of the binormal distribution of galaxies in each luminosity bin. The solid dots indicate the corresponding averages of the two Gaussian peaks. The solid line is the best-fit quadratic relation to these averages (see eq. [1]), which we use to split the galaxies into red and blue population (color-coded accordingly).

the CLFs for all, red and blue galaxies. Sections 4, 5 and 6 describe the properties of central galaxies, the halo occupation statistics and the fraction of satellite galaxies, respectively. Finally, we summarize our results in Section 7. Throughout this paper, we use a Λ CDM ‘concordance’ cosmology whose parameters are consistent with the three-year data release of the WMAP mission: $\Omega_m = 0.238$, $\Omega_\Lambda = 0.762$, $n_s = 0.951$, $h = 0.73$ and $\sigma_8 = 0.75$ (Spergel et al. 2007).

2. DATA

The analysis presented in this paper is based on the SDSS DR4 galaxy group catalogue constructed by Y07 using an adaptive halo-based group finder (Yang et al. 2005a). The related galaxy catalogue is the New York University Value-Added Galaxy Catalogue (NYU-VAGC; Blanton et al. 2005b), which is based on the SDSS Data Release 4 (Adelman-McCarthy et al. 2006), but with an independent set of significantly improved reductions. From this catalogue we select all galaxies in the Main Galaxy Sample with redshifts in the range $0.01 \leq z \leq 0.20$ and with a redshift completeness $\mathcal{C} > 0.7$. As described in Y07, three group samples were constructed from the corresponding galaxy samples: Sample I, which only uses the 362356 galaxies with measured r -band magnitudes and redshifts from the SDSS, Sample II which also includes 7091 galaxies with SDSS r -band magnitudes but redshifts taken from alternative surveys, and Sample III which includes an additional 38672 galaxies that lack redshifts due to fiber collisions but that are assigned the redshifts of their nearest neighbors (cf. Zehavi et al. 2002). Unless stated otherwise, our analysis is based on Sample II. For comparison, we also present some results obtained from Sample III.

The magnitudes and colors of all galaxies are based on the standard SDSS Petrosian technique (Petrosian 1976; Strauss et al. 2002), have been corrected for galactic extinction (Schlegel, Finkbeiner & Davis 1998), and have

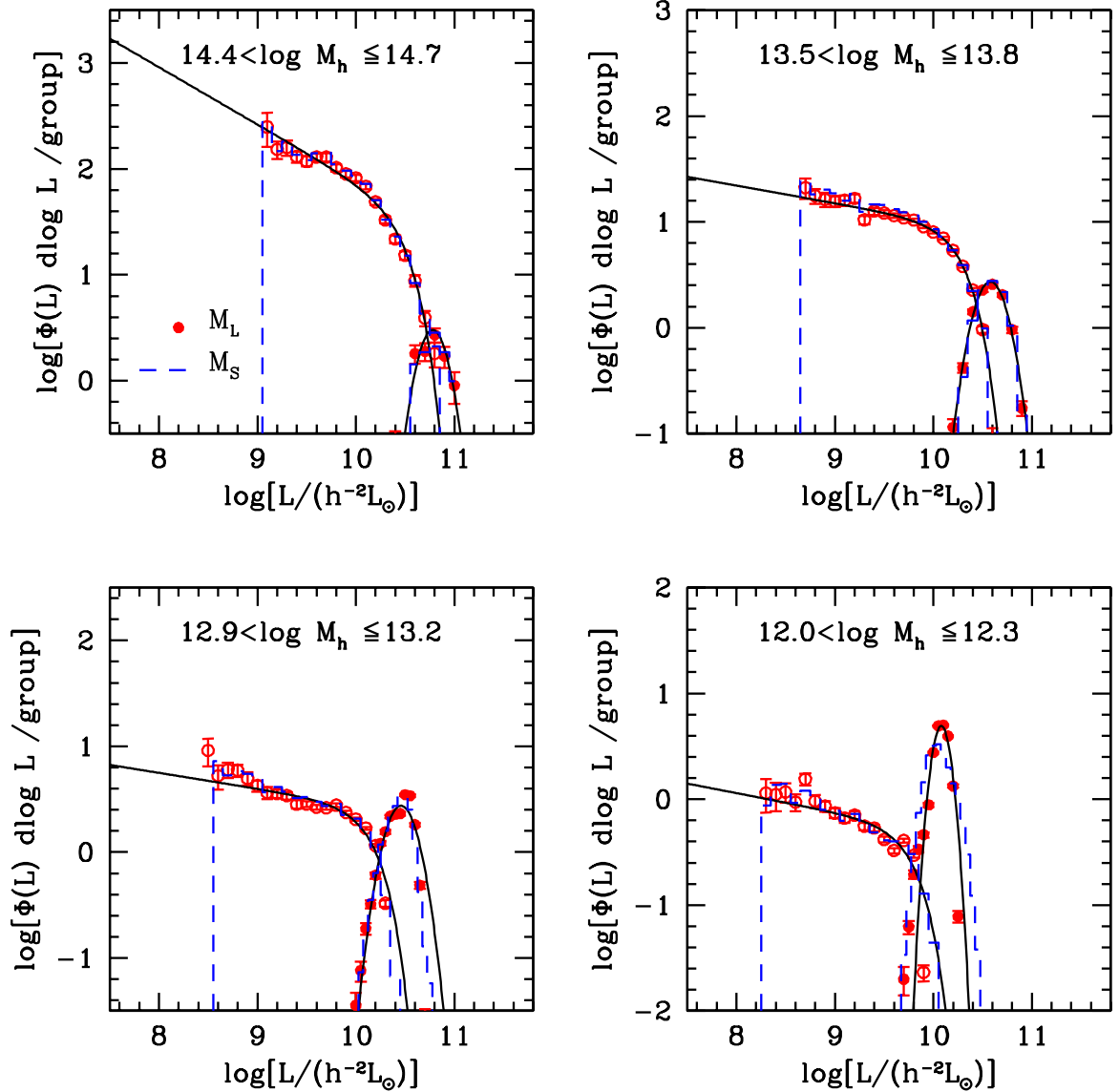


FIG. 2.— The conditional luminosity functions (CLFs) of galaxies in groups of different mass bins. Symbols correspond to the CLFs obtained using M_L as halo mass (estimated according to the ranking of the characteristic group luminosity), with solid and open circles indicating the contributions from central and satellite galaxies, respectively. The errorbars reflect the $1\text{-}\sigma$ scatter obtained from 200 bootstrap samples. The solid lines indicate the related best-fit parameterizations using equation [2]. For comparison, we also show, with dashed lines, the CLFs obtained using M_S as halo mass (estimated according to the ranking of the group's characteristic stellar mass). Results shown in this plot are obtained from Sample II.

been K -corrected and evolution corrected to $z = 0.1$, using the method described in Blanton et al. (2003a, b). We use the notation $^{0.1}M_r$ to indicate the resulting absolute magnitude in the r -band. Stellar masses, indicated by M_* , for all galaxies are computed using the relations between stellar mass-to-light ratio and $^{0.1}(g-r)$ color of Bell et al. (2003; see Y07 for details).

In this study we separate galaxies into red and blue subsamples according to their bi-normal distribution in the $^{0.1}(g-r)$ color (Baldry et al. 2004; Blanton et al. 2005a; Li et al. 2006). Fig. 1 shows the color-magnitude distribution of the galaxies in our Sample II (dots) together with the two peak values of the bi-normal distribution in each absolute magnitude bin (open circles) (Cheng Li; private communication). The galaxies are separated into red and blue subsamples using the

solid line, which is the best fit to the average of the two peak values in each absolute magnitude bin:

$$^{0.1}(g-r) = 1.022 - 0.0651x - 0.00311x^2, \quad (1)$$

where $x = ^{0.1}M_r - 5 \log h + 23.0$.

For each group in our catalogue we have two estimates of its dark matter halo mass M_h : (1) M_L , which is based on the ranking of the characteristic group luminosity $L_{19.5}$, and (2) M_S , which is based on the ranking of the characteristic group stellar mass M_{stellar} , respectively⁵. As shown in Y07, these two halo masses agree reasonably well with each other, with a scatter that decreases from ~ 0.1 dex at the low-mass end to ~ 0.05 dex at the

⁵ $L_{19.5}$ and M_{stellar} are, respectively, the total luminosity and total stellar mass of all group members with $^{0.1}M_r - 5 \log h \leq -19.5$.

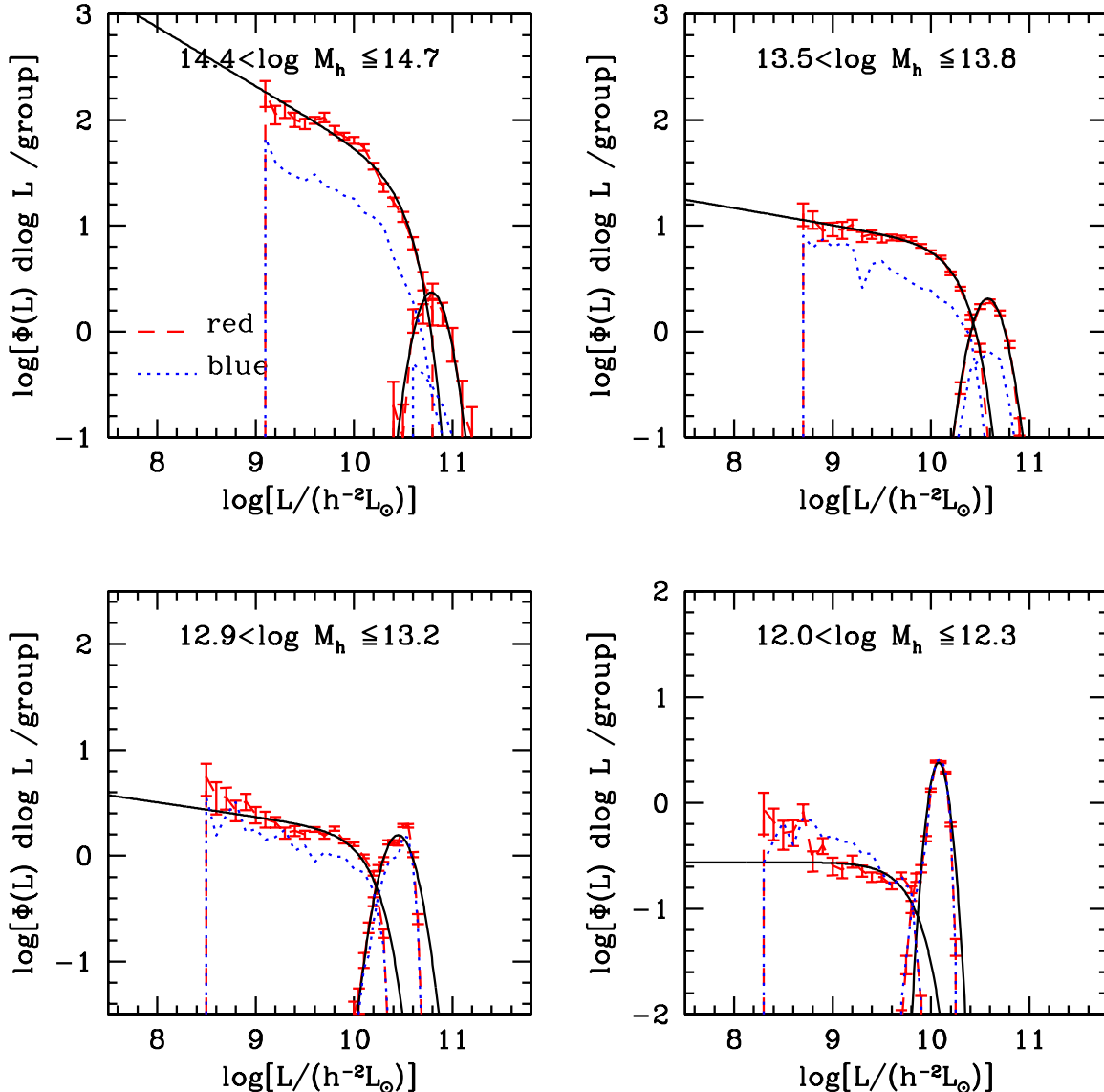


FIG. 3.— Similar to Fig. 2, but here we show the CLFs for red (dashed lines) and blue (dotted lines) galaxies, for groups with halo masses M_L . The solid lines indicate the best-fit parameterizations for the CLFs of red galaxies. In both cases the central and satellite components of the CLFs are indicated separately. For clarity, the errorbars, again obtained using 200 bootstrap samples, are only shown for the red galaxies.

massive end. Detailed tests using mock galaxy redshift surveys have demonstrated that the group masses thus estimated can recover the true halo masses with a $1-\sigma$ deviation of ~ 0.3 dex, and are more reliable than those based on the velocity dispersion of group members (Y05; Weinmann et al. 2006; Berlind et al. 2006; Y07). Note also that survey edge effects have been taken into account in our group catalogue: groups that suffer severely from edge effects (about 1.6% of the total) have been removed from the catalogue. In most cases, we take the brightest galaxy in the group as the central galaxy (BCG) and all others as satellite galaxies. In addition, we also considered a case in which the most massive galaxy (in terms of stellar mass) in a group is considered as the central galaxy (MCG). Tests have shown that for most of what follows, these two definitions yield indistinguishable results. Whenever the two definitions lead to significant differences, we present results for both.

3. THE CONDITIONAL LUMINOSITY FUNCTIONS FOR ALL, RED AND BLUE GALAXIES

The conditional luminosity function (CLF) of galaxies in dark halos, $\Phi(L|M)$, which describes the average number of galaxies as a function of galaxy luminosity in a dark matter halo of a given mass, plays an important role in our understanding of how galaxies form in dark matter halos (Yang, Mo & van den Bosch 2003; van den Bosch, Yang & Mo; 2003; Cooray 2006; Vale & Ostriker 2006; van den Bosch et al. 2007a). We now use our group catalogue to directly determine $\Phi(L|M)$.

The CLF can be estimated by directly counting galaxies in groups. For a given galaxy luminosity L , there is a limiting redshift, z_L , beyond which galaxies with such a luminosity are not included in the sample. As discussed in Y07, the group catalogue is complete to a certain limiting redshift for a given halo mass. In order to estimate the CLF, $\Phi(L|M)$ at a given L , we only use

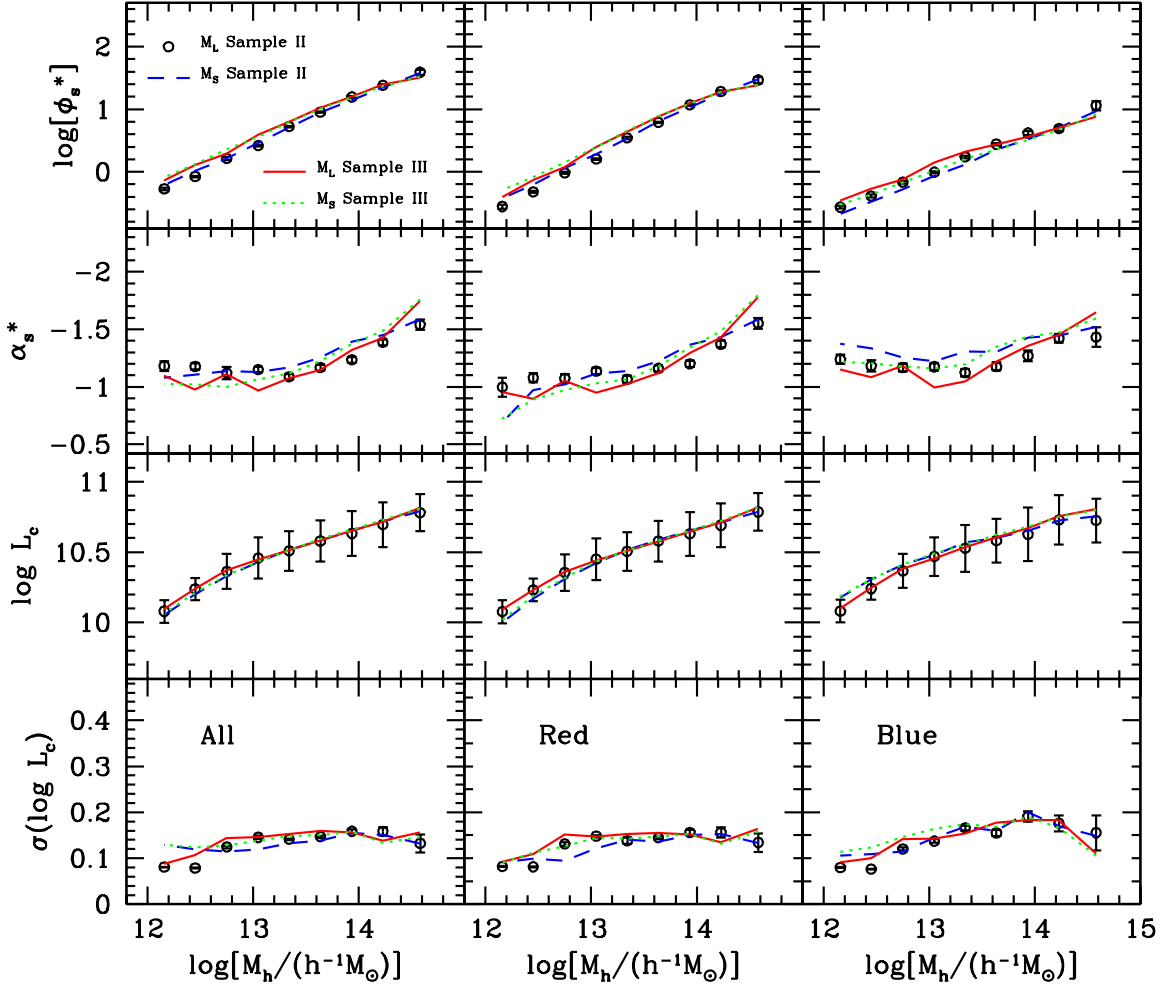


FIG. 4.— The best fit parameters (ϕ_s^* upper row, α_s^* second row, L_c third row, and σ_c bottom row) to the CLFs shown in Figs. 2 and 3, as functions of halo mass. Panels on the left, in the middle, and on the right show results for all, red, and blue galaxies, respectively. Since we have two different halo mass estimators (M_L and M_S) and two main group samples (II and III), we have obtained CLFs for four different combinations of sample and group mass estimator. The results for all four combinations are shown using different symbols and line-styles, as indicated. The errorbars in the first two and last rows indicate the $1-\sigma$ variances obtained from our 200 bootstrap samples. In the third row of panels, however, the errorbars correspond to the log-normal scatter, σ_c , shown in the bottom row of panels. For clarity the errorbars are only shown for the ' M_L -Sample II' case, but they are very similar for the other four cases.

groups that are complete to the redshift limit z_L . The CLF is obtained by simply counting the average number of galaxies (in luminosity bins) in groups of a given M . We show in Fig. 2 the resulting CLFs for groups of different masses. The contributions of central and satellite galaxies are plotted separately. For comparison, results obtained using both M_L and M_S are shown as symbols and dashed lines, respectively. Overall, these two halo masses give consistent results, except that the M_L -based CLF of the central galaxies in low mass halos is more peaked than the M_S -based CLF (see the lower right-hand panel). The errorbars shown in each panel correspond to $1-\sigma$ scatter obtained from 200 bootstrap samples of our group catalogue. The CLF for the total population (centrals plus satellites) matches reasonably well the Schechter form down to halo masses of $M \sim 10^{13.5} h^{-1} M_\odot$. For less massive halos, however, there is a prominent peak in the CLF at the bright end due to the contribution of central galaxies, which makes the total CLF deviate significantly from the Schechter form. As discussed in Y05c, in low-mass halos where the

group characteristic luminosity ($L_{19.5}$) is dominated by the central galaxy, the $L_{19.5}$ - M_L conversion can produce an artificial peak in the CLF at the bright end. However, comparing the results obtained here with the test results shown in Fig. 9 of Y05c indicates that the strong peak in the lower right panel of Fig. 2 cannot be entirely due to the $L_{19.5}$ - M_L conversion. Therefore, in what follows, we will model the CLF for central and satellite galaxies separately.

Fig. 3 shows the CLFs separately for red (dashed lines) and blue (dotted lines) galaxies. Note that massive halos clearly contain more red galaxies than blue galaxies (both centrals and satellites), while the opposite applies to low mass halos. The overall CLF shapes for red and blue galaxies, however, are remarkably similar.

To quantify the CLFs, we fit each of them with the following model. We write the total CLF as the sum of the CLFs of central and satellite galaxies:

$$\Phi(L|M) = \Phi_{\text{cen}}(L|M) + \Phi_{\text{sat}}(L|M). \quad (2)$$

We assume the contribution from the central galaxies to

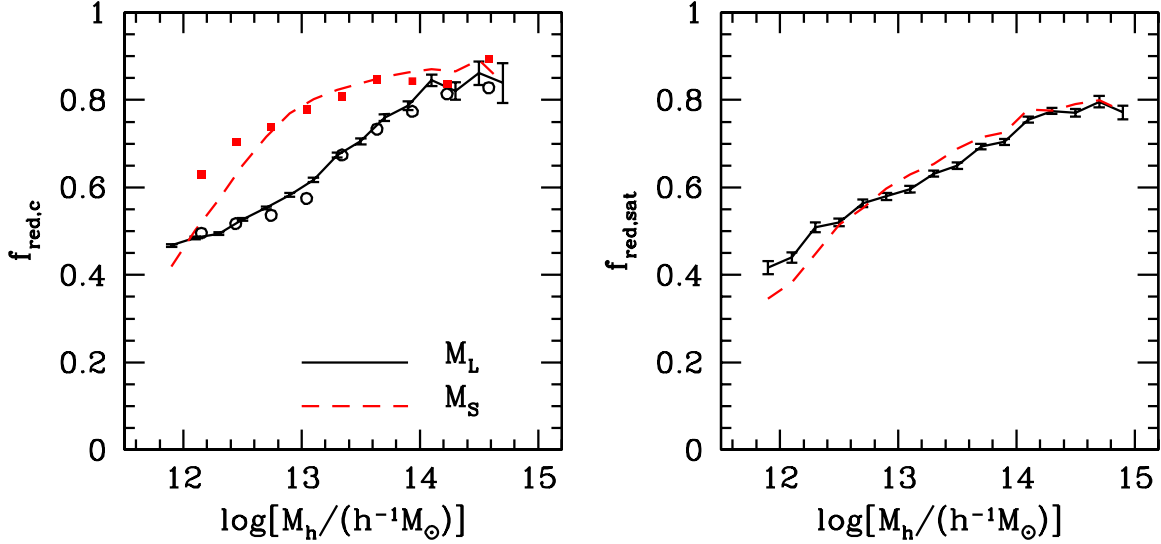


FIG. 5.— Fraction of red galaxies among central (left-hand panel) and satellite (right-hand panel) galaxies. Solid and dashed lines show results for groups with halo mass estimators M_L and M_S , respectively. For comparison, we show also the fractions of red central galaxies obtained from the CLFs (Eq. 3) as open circles (for M_L) and solid squares (for M_S). Errorbars (shown only for M_L) are obtained from the 200 bootstrap samples. See text for a detailed discussion.

be a lognormal:

$$\Phi_{\text{cen}}(L|M) = \frac{A}{\sqrt{2\pi}\sigma_c} \exp \left[-\frac{(\log L - \log L_c)^2}{2\sigma_c^2} \right], \quad (3)$$

where A is the number of central galaxies per halo. Thus, $A \equiv 1$ for all galaxies, $A = f_{\text{red}}$ (with f_{red} being the fraction of red central galaxies) for red galaxies, and $A = 1 - f_{\text{red}}$ for blue galaxies. Note that $\log L_c$ is, by definition, the expectation value for the (10-based) logarithm of the luminosity of the central galaxy;

$$\log L_c = \int_0^\infty \Phi_{\text{cen}}(L|M) \log L dL, \quad (4)$$

and that $\sigma_c = \sigma(\log L_c)$. For the contribution from the satellite galaxies we adopt a modified Schechter function:

$$\Phi_{\text{sat}}(L|M) = \phi_s^* \left(\frac{L}{L_s^*} \right)^{(\alpha_s^*+1)} \exp \left[-\left(\frac{L}{L_s^*} \right)^2 \right]. \quad (5)$$

Note that this function decreases faster at the bright end than a Schechter function. This CLF parameterization has a total of five free parameters: L_c , σ_c , ϕ_s^* , α_s^* and L_s^* . In practice, we find that $\log L_c \sim \log L_s^* + 0.25$ to good approximation. We therefore adopt $\log L_c \equiv \log L_s^* + 0.25$, throughout, which reduces the number of free parameters to four.

For all the CLFs measured above, the best fit parameters, using the model described by equation 2, are shown in Fig. 4. Results are shown separately for all (left column panels), red (middle column panels) and blue (right column panels) galaxies. The error-bars in the upper two rows reflect the $1-\sigma$ scatter obtained from our 200 bootstrap samples. Here we also compare results obtained using Samples II and III. Note that Sample II does not include any galaxies missed due to fiber collisions, while Sample III includes all such galaxies by assigning each of them the redshift of its nearest neighbor. Although this fiber collision correction works well in roughly 60 percent

of all cases, the remaining 40 percent are assigned redshifts that can be very different from their true values (Zehavi et al. 2002). Samples II and III should therefore be considered as two extremes as far as a treatment of fiber-collisions is concerned. Given that we also have two kinds of halo masses, M_L and M_S , we have a total of four different combinations for which we have determined the CLF. The results for all four cases are shown as different symbols in each of the panels of Fig. 4. As an illustration of how well the model fits the data, the solid lines in Figs. 2 and 3 indicate the corresponding best-fit models.

The upper row of Fig. 4 shows the best fit normalization of the CLF for satellite galaxies, which describes the average number of satellite galaxies with luminosity $\sim L_s^*$ in a group of a given halo mass. As expected, Sample III gives a higher ϕ_s^* , especially for low-mass groups. Comparing ϕ_s^* for red (upper middle panel) and blue (upper right panel) galaxies, one sees that the fraction of red satellites increases with halo mass. The second row shows the faint end slopes of the CLFs, α_s^* . In massive halos with $M_h \gtrsim 10^{13} h^{-1} M_\odot$, α_s^* decreases (i.e., becomes more negative) with increasing halo mass, both for red and for blue galaxies. In halos with $M_h \lesssim 10^{13} h^{-1} M_\odot$, however, α_s^* decreases with increasing halo mass for red satellites, but increases with M_h for blue satellites, while the faint-end slope for the entire satellite population (red and blue combined) is roughly constant at ~ -1.1 . The third row of panels shows that $\log L_c$ increases with halo mass, for both red and blue centrals. A more detailed discussion regarding this and other properties of central galaxies will be presented in Section 4). Finally, the last row of Fig 4 shows the width of the log-normal CLF of central galaxies. For the combined sample of red and blue galaxies we find an average value of $\sigma_c = \sigma(\log L_c) \sim 0.15$. This is in good agreement with constraints obtained by Yang et al. (2003) and Cooray (2006) from clustering and abundances of galaxies in the 2dFGRS and SDSS, respectively. However, Zheng et al. (2007) found, based on HODs models for the SDSS and DEEP2, that the

log-normal width increases from ~ 0.13 for massive halos with $M_h \sim 10^{13.5} h^{-1} M_\odot$ to ~ 0.3 for low mass halos with $M_h \sim 10^{11.5} h^{-1} M_\odot$. This is quite different from our results, which suggest that $\sigma(\log L_c)$ decreases with decreasing halo mass. However, this is most likely an artefact of the method that we used to assign halo masses to our groups. As mentioned above, our halo masses are based on the ranking of either $L_{19.5}$ or M_{stellar} , which implies that we have assumed a one-to-one relation between halo mass and these two indicators. At the low mass end, both $L_{19.5}$ and M_{stellar} are expected to be strongly correlated with the luminosity of corresponding central galaxies. Therefore the values of σ_c obtained here should be considered as lower limits, in particular for low mass halos.

For reference, Table 1 lists the *average* values of the CLF fitting parameters obtained from the four combinations of Samples II and III and group masses M_L and M_S . The errorbars indicate the scatter among these four combinations or the scatter obtained from the 200 bootstrap samples, whichever is larger.

As shown in Weinmann et al. (2006b) and Baldry et al. (2006), the red and blue fractions of galaxies as function of halo mass provide important constraints for models of galaxy formation. Fig. 5 shows the red fractions of centrals (left-hand panel) and satellites (right-hand panel) as function of halo mass obtained from our group catalogue (solid and dashed lines). These fractions are obtained by simply dividing the number of red centrals (satellites) by the number of all centrals (satellites) in a given halo mass bin. For both centrals and satellites the red fraction increases with increasing halo mass. For comparison, results are shown for both M_L (solid lines) and M_S (dashed lines). These two different halo mass estimates give quite different results for central galaxies, especially for halos with $M_h \sim 10^{13} h^{-1} M_\odot$. The origin of this discrepancy can be understood in terms of Fig. 1. In this color-magnitude diagram, the galaxies are separated into red and blue populations. If we would convert this color-magnitude diagram into a color-stellar mass diagram, the red and blue populations would shift slightly towards higher and lower stellar masses, respectively (according to the Eq. 2 in Y07). Therefore, a certain upper percentile of galaxies that is ranked according to stellar mass will have a larger red fraction than the same percentile ranked according to luminosity. Because of the tight correlation between the luminosity of the central galaxy and M_L , and between the stellar mass of the central galaxy and M_S , it is clear that centrals in a given bin of M_S have a larger red fraction than those in the same bin of M_L .

We can also determine the red fractions of centrals from our best-fit CLF parameterizations (equation [3]). As shown above, the parameterization of $\Phi_{\text{cen}}(L|M)$ involves the parameter f_{red} , which describes the fraction of central galaxies that are red. For comparison, the symbols in the left-hand panel of Fig. 5 show the best-fit values of f_{red} obtained from the CLFs for the M_L masses (open circles) and M_S masses (solid squares). It is reassuring that these best fit results match the direct determination of the red fractions reasonably well. The small differences between the direct measurement (lines) and CLF measurement (symbols) owe to the fact that in the latter case we have normalized the galaxies using

the number of groups within the redshift limit z_L (see Section 3).

The results shown in the left panel indicate that more than 80% of the central galaxies in halos more massive than $\sim 10^{14} h^{-1} M_\odot$ are red galaxies, while in smaller halos with masses $\sim 10^{12} h^{-1} M_\odot$, less than 50% of the centrals are red. As discussed in Y07, M_S may represent the true halo mass better than M_L . The result based on M_S shows that f_{red} decreases rapidly with decreasing halo mass at $M_h \lesssim 10^{13} h^{-1} M_\odot$. The right panel of Fig. 5 shows the fraction of red satellite galaxies as a function of halo mass. As one can see, for satellite galaxies f_{red} increase steadily from about 40% for halos with $M_h \sim 10^{12} h^{-1} M_\odot$ to about 80% in massive halos with $M_h \sim 10^{15} h^{-1} M_\odot$. In van den Bosch et al. (2007b) we have used this information to constrain the efficiency with which the star formation of galaxies is quenched once they become a satellite galaxy (i.e., after they are accreted into a larger halo).

4. THE PROPERTIES OF CENTRAL GALAXIES

We now turn to a more detailed investigation of the properties of central galaxies in our group catalogue. We re-iterate that a central galaxy is either defined as the brightest group member (BCG) or the most massive group member (MCG).

4.1. Central luminosity (stellar mass) - halo mass relation

In Fig. 6, we show the luminosity - halo mass (left panel) and stellar mass - halo mass (right panel) relations. The solid circles and shaded areas indicate the median and 68% confidence levels of these relations obtained using M_L as halo mass, while the open squares with error-bars are the results obtained using M_S as halo mass. Clearly, and not surprisingly, the luminosity (stellar mass) of the BCG (MCG) increases with halo mass. In both cases we find that the slope of the relation decreases significantly with increasing halo mass, in good agreement with previous results (e.g., Vale & Ostriker 2004, 2006; Cooray 2005; Yang et al. 2003; Y05c; van den Bosch et al. 2007a). The physical reason for this change in slope is probably a combination of AGN feedback, and changes in the efficiencies of radiative cooling and dynamical friction (e.g. Lin et al. 2004; Dekel 2004; Cooray & Milosavljević 2005).

To quantify the $L_c - M_h$ relation shown in the left panel, we fit the data using the following function,

$$L_c = L_0 \frac{(M_h/M_1)^{\alpha+\beta}}{(1 + M_h/M_1)^\beta}. \quad (6)$$

This model contains four free parameters: a normalized luminosity, L_0 , a characteristic halo mass, M_1 , and two slopes, α and β . The solid line shown in the left panel is the best fit to the average $L_c - M_h$ relation. Note that using M_L or M_S as the halo mass does not lead to any significant changes in the results. The best fitting parameters are $[\log L_0, \log M_1, \alpha, \beta] = [10.45, 12.54, 0.17, 0.51]$. Thus, according to Eq. 6, L_c scales with M_h roughly as $L_c \propto M_h^{0.17}$ for halos with $M_h \gg 10^{12.5} h^{-1} M_\odot$, and as $L_c \propto M_h^{0.68}$ for halos with $M_h \ll 10^{12.5} h^{-1} M_\odot$. Unfortunately, since we do not have data for halos with

TABLE 1
THE BEST FIT PARAMETERS OF CLFs FOR ALL, RED AND BLUE GALAXIES

Galaxy	$\log[M_h]$	$\log\langle[M_h]\rangle$	ϕ_s^*	α_s^*	$\log L_c$	σ_c
(1)	(2)	(3)	(4)	(5)	(6)	(7)
ALL	[14.40, 15.00]	14.58	35.51 ± 3.88	-1.66 ± 0.11	10.799 ± 0.019	0.141 ± 0.021
	[14.10, 14.40]	14.23	23.68 ± 1.07	-1.44 ± 0.04	10.714 ± 0.014	0.146 ± 0.011
	[13.80, 14.10]	13.94	15.27 ± 0.90	-1.33 ± 0.07	10.649 ± 0.012	0.157 ± 0.005
	[13.50, 13.80]	13.64	9.60 ± 0.82	-1.20 ± 0.05	10.584 ± 0.006	0.149 ± 0.009
	[13.20, 13.50]	13.34	5.72 ± 0.60	-1.11 ± 0.04	10.513 ± 0.003	0.144 ± 0.009
	[12.90, 13.20]	13.05	3.27 ± 0.60	-1.08 ± 0.08	10.442 ± 0.013	0.137 ± 0.012
	[12.60, 12.90]	12.75	1.87 ± 0.29	-1.09 ± 0.06	10.350 ± 0.020	0.128 ± 0.012
	[12.30, 12.60]	12.45	1.12 ± 0.23	-1.07 ± 0.09	10.224 ± 0.019	0.107 ± 0.020
RED	[12.00, 12.30]	12.16	0.67 ± 0.12	-1.10 ± 0.06	10.074 ± 0.018	0.107 ± 0.026
	[14.40, 15.00]	14.58	27.14 ± 3.25	-1.68 ± 0.13	10.801 ± 0.022	0.147 ± 0.021
	[14.10, 14.40]	14.23	18.72 ± 2.53	-1.43 ± 0.07	10.709 ± 0.051	0.144 ± 0.029
	[13.80, 14.10]	13.94	11.79 ± 0.76	-1.30 ± 0.07	10.644 ± 0.011	0.153 ± 0.006
	[13.50, 13.80]	13.64	6.98 ± 0.80	-1.17 ± 0.04	10.581 ± 0.005	0.146 ± 0.008
	[13.20, 13.50]	13.34	3.97 ± 0.59	-1.07 ± 0.05	10.510 ± 0.008	0.144 ± 0.007
	[12.90, 13.20]	13.05	2.12 ± 0.44	-1.06 ± 0.09	10.438 ± 0.011	0.140 ± 0.012
	[12.60, 12.90]	12.75	1.18 ± 0.19	-1.03 ± 0.04	10.335 ± 0.026	0.126 ± 0.023
BLUE	[12.30, 12.60]	12.45	0.67 ± 0.15	-0.96 ± 0.09	10.207 ± 0.031	0.100 ± 0.014
	[12.00, 12.30]	12.16	0.39 ± 0.09	-0.84 ± 0.16	10.046 ± 0.046	0.089 ± 0.005
	[14.40, 15.00]	14.58	9.21 ± 1.98	-1.55 ± 0.09	10.770 ± 0.043	0.130 ± 0.045
	[14.10, 14.40]	14.23	4.94 ± 0.57	-1.45 ± 0.05	10.740 ± 0.024	0.174 ± 0.019
	[13.80, 14.10]	13.94	3.59 ± 0.42	-1.37 ± 0.08	10.658 ± 0.024	0.191 ± 0.012
	[13.50, 13.80]	13.64	2.51 ± 0.27	-1.26 ± 0.08	10.603 ± 0.017	0.165 ± 0.011
	[13.20, 13.50]	13.34	1.69 ± 0.34	-1.17 ± 0.11	10.546 ± 0.019	0.166 ± 0.009
	[12.90, 13.20]	13.05	1.08 ± 0.24	-1.14 ± 0.10	10.473 ± 0.016	0.147 ± 0.011
	[12.60, 12.90]	12.75	0.66 ± 0.10	-1.20 ± 0.06	10.392 ± 0.022	0.131 ± 0.015
	[12.30, 12.60]	12.45	0.43 ± 0.08	-1.20 ± 0.10	10.277 ± 0.037	0.102 ± 0.020
	[12.00, 12.30]	12.16	0.28 ± 0.06	-1.25 ± 0.09	10.135 ± 0.052	0.098 ± 0.015

NOTE. — Column (1): Galaxy sample. Column (2): halo mass range. Column (3): average of the logarithm of the halo mass. Column (4)-(7): average of the best fit free parameters to the four measurements of the CLFs, as shown in Fig. 4. The errors indicate the scatter among these four measurements or the scatter obtained from the 200 bootstrap samples, whichever is larger.

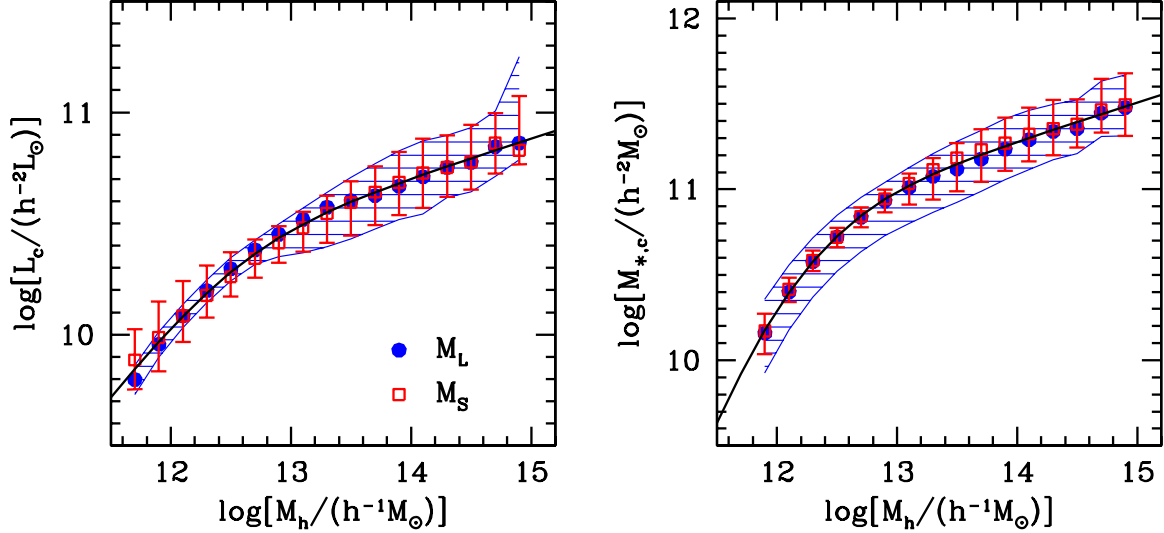


FIG. 6.— The left-hand panel shows the median luminosity of the BCG, L_c , as function of halo mass, M_h . The solid dots and open squares show the results for halo mass M_L and M_S , respectively. The related shaded areas (or error-bars) show the 68% confidence regions of L_c . The right-hand panel shows the median stellar mass of the MCG, $M_{*,c}$, as function of halo mass, M_h . Again solid dots and open squares show the results for halo mass M_L and M_S , and shaded area (or error-bars) show the 68% confidence regions of $M_{*,c}$. The solid lines shown in the left and right panels are the best fit results using equations 6 and 7, respectively.

$M_h < 10^{11.6} h^{-1} M_\odot$, any change of behavior at the low-mass end is not constrained. For the $M_{*,c} - M_h$ relation shown in the right panel, we use a similar function to fit the data:

$$M_{*,c} = M_0 \frac{(M_h/M_1)^{\alpha+\beta}}{(1 + M_h/M_1)^\beta}. \quad (7)$$

The solid line shown in the right panel is the best fit of this model to the data, and the best-fit parameters are $[\log M_0, \log M_1, \alpha, \beta] = [10.86, 12.08, 0.22, 1.61]$. Thus, $M_{*,c}$ scales with M_h as $M_{*,c} \propto M_h^{0.22}$ for halos with $M_h \gg 10^{12.1} h^{-1} M_\odot$, and as $M_{*,c} \propto M_h^{1.83}$ for halos with $M_h \ll 10^{12.1} h^{-1} M_\odot$.

4.2. The luminosity (stellar mass)-gap statistic

An useful quantity to describe the difference between the central and satellite galaxies is the so-called ‘luminosity-gap’ between the BCG and the brightest satellite galaxy in a given halo. This ‘luminosity-gap’ holds important information regarding the formation and evolution of galaxies. For example, as discussed in D’Onghia et al. (2005) and Milosavljević et al. (2006), the luminosity-gap may be used to quantify the dynamical age of a system of galaxies: halos with L_2/L_1 close to unity must be relatively young, as dynamical friction causes multiple luminous galaxies in the same halo to merge on a relatively short time scale. Put differently, the distribution of L_2/L_1 holds important information regarding the importance of galactic cannibalism for BCGs (e.g., Tremaine & Richstone 1977; Vale & Ostriker 2007).

Using our group catalogue, it is straightforward to measure L_2/L_1 , as well as the stellar mass equivalent, $M_{*,2}/M_{*,1}$, as function of group mass, as long as the group has at least two members. In the case of ‘isolated galaxies’, i.e., groups with only one member (the central), however, there are two possibilities: either the galaxy is truly isolated, in that its halo contains no satellite galaxies, or the halo contains one or more satellite galaxies that are fainter than the flux limit of the survey. To bracket the extremes we proceed as follows. For isolated galaxies we either assume that the brightest satellite has zero luminosity (case 1) or that its luminosity is such that its apparent magnitude limit is equal to the magnitude limit of our sample (case 2). Fig. 7 shows the results thus obtained for both the luminosity gap (left-hand panel) and the stellar mass gap (right-hand panel). Symbols and shaded areas indicate the medians and 68% confidence intervals, respectively, and results are shown for both case 1 (open squares) and case 2 (solid dots). For groups with $M_h \gtrsim 10^{13.5} h^{-1} M_\odot$, case 1 and 2 yield identical results, simply because all these groups contain at least two member galaxies above the magnitude limit of the survey. In the most massive halos, with $M_h \gtrsim 10^{14.5} h^{-1} M_\odot$, the median gap is $\log L_1 - \log L_2 \sim \log M_1 - \log M_2 \sim 0.2$. The median luminosity or stellar mass gap can be reliably measured down to a halo masses of $M_h \sim 10^{13.5} h^{-1} M_\odot$, where the median values are $\log L_1 - \log L_2 \sim 0.3$ and $\log M_1 - \log M_2 \sim 0.4$. For halos with $M_h \lesssim 10^{13.5} h^{-1} M_\odot$, however, cases 1 and 2 yield very different results, indicating that the flux limit of the survey severely impedes our ability to accurately measure the gap statistics. Finally we emphasize that

the luminosity-gap statistics obtained from Samples II and III separately are very similar, indicating that fiber collisions do not have a strong impact on the results presented here.

As pointed out by Tremaine & Richstone (1977; and references therein), the ‘luminosity-gap’ can be used to determine whether the BCGs in galaxy groups are statistically drawn from the same distribution as the satellite galaxies or whether they are ‘special’. If the average magnitude difference between the BCGs and the brightest satellite galaxies is smaller than the standard deviation in the magnitudes of the BCGs, then they are consistent with being drawn from the same distribution. To test this, the solid curve in the left-hand panel of Fig. 7 indicates the best-fit values of $\sigma_c = \sigma(\log L_c)$ obtained from the CLFs. A comparison with the median luminosity gaps suggests that the BCGs in groups, especially with $M_h \lesssim 10^{14.0} h^{-1} M_\odot$, form a ‘special’ subclass, in that their luminosities can not be considered the extreme values of the distribution of satellite luminosities. As a cautionary remark, we emphasize that because of the method used to assign halo masses to the groups, the value of σ_c may be underestimated, especially for low mass groups (see discussion in section 3). However, even if σ_c were underestimated by a factor two at the low mass end, this would not change our conclusion that BCGs are special in low mass halos.

The ‘luminosity-gap’ can also be described using its distribution for groups of a given mass. In the upper panels of Fig. 8 we show the distribution of $\log L_1 - \log L_2$ for groups in the above mentioned case 1 (unshaded histograms) and case 2 (shaded histograms), respectively. Results are shown for three different mass bins, as indicated in the panels. In the lower panels of Fig. 8, results are shown for the corresponding stellar mass gap distributions. One can see, the width of the distribution increases with decreasing halo mass.

Systems with a relatively large luminosity gap, which most likely owes to the fact that the brightest galaxies in the halo have merged, are often termed “fossil groups” and have received a significant amount of attention in the recent literature (see Vikhlinin et al. 1999; Jones et al. 2003; D’Onghia et al. 2005; Milosavljević et al. 2006; Sommer-Larsen 2006; van den Bosch et al. 2007a; Sales et al. 2007; von Benda-Beckmann et al. 2007). Following Jones et al. (2003) and Milosavljević et al. (2006) we define systems in which the brightest satellite galaxy is at least 2 magnitudes fainter than the BCG (i.e., $\log L_1 - \log L_2 \geq 0.8$, indicated as the dotted vertical lines in Fig. 8), as “fossil” systems. From the SDSS DR4 group catalogue, we obtain that the fraction of fossil systems increases from ~ 0.5 percent for groups with $M_h \sim 10^{14.5} h^{-1} M_\odot$, to ~ 2.5 percent for groups with $M_h \sim 10^{14.0} h^{-1} M_\odot$, 11 – 20 percent for groups with $M_h \sim 10^{13.5} h^{-1} M_\odot$, and 18 – 60 percent for groups with $M_h \sim 10^{13.0} h^{-1} M_\odot$ ⁶. These results are in good agreement with a similar analysis of galaxy groups in the 2dFGRS by van den Bosch et al. (2007a). On the other hand, Jones et al. (2003) obtained an incidence rate of 8 to 20 percent for systems with an X-ray luminosity from diffuse, hot gas of $L_{X,\text{bol}} \geq 2.5 \times 10^{41} h^{-2} \text{ergs}^{-1}$.

⁶ Whenever two values are quoted, these reflect the two extreme cases described above.

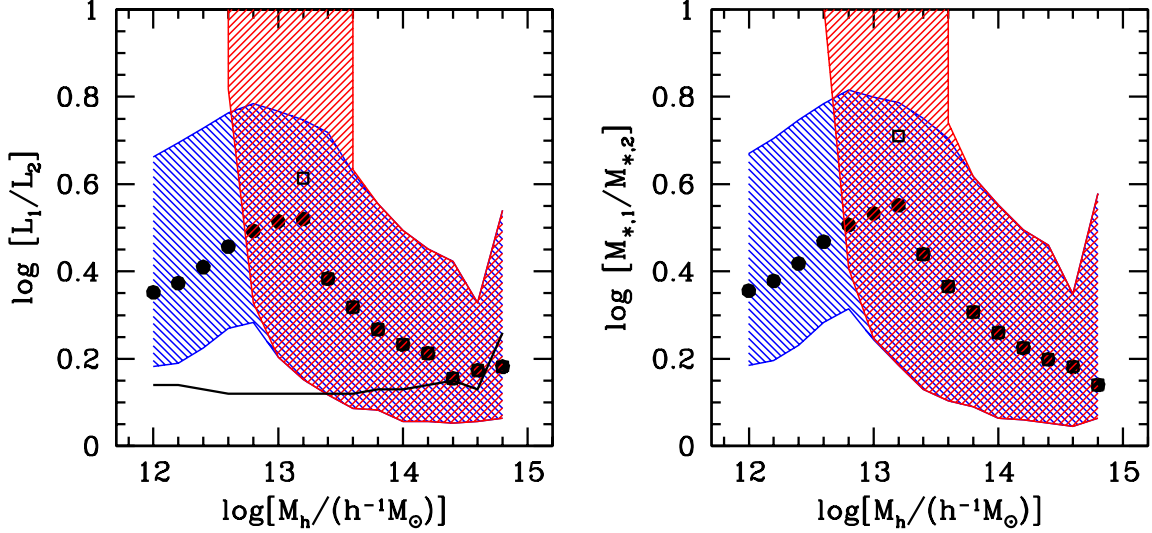


FIG. 7.— The left-hand panel shows the luminosity gap between the BCG and the brightest satellite galaxy in the group, $\log L_1 - \log L_2$, as function of group mass M_h . The right-hand panel shows the stellar mass gap between the MCG and the most massive satellite galaxy, $\log M_{*,1} - \log M_{*,2}$ as function of group mass M_h . Results are shown for two cases, where groups with only 1 member are treated differently. In case 1, we assume that the brightest satellite galaxy has zero luminosity (open squares), while in case 2 we assume that the brightest satellite galaxy has an apparent magnitude equal to the magnitude limit of the survey (solid dots). The shaded areas indicate the corresponding 68% confidence intervals. The solid line in the left panel shows the best fit values of $\sigma(\log L_c)$ obtained from the CLFs.

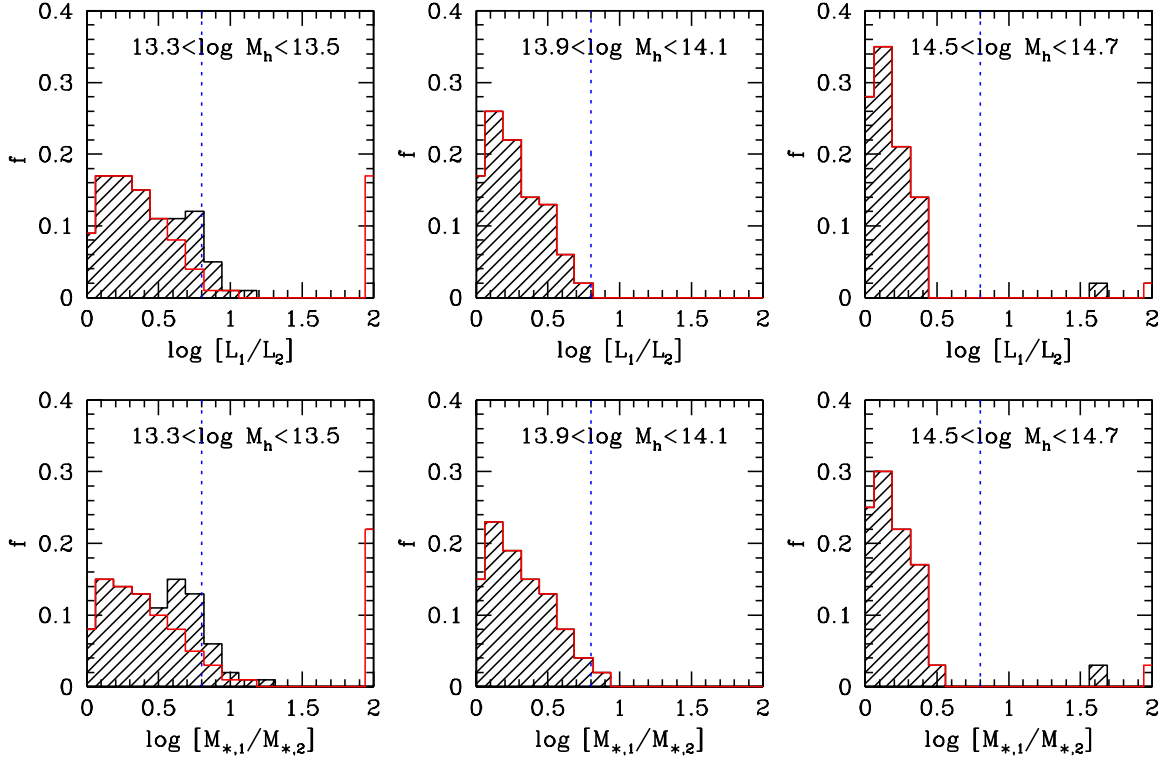


FIG. 8.— The probability distributions of luminosity gap $\log L_1 - \log L_2$ (upper panels) and stellar mass gap $\log M_{*,1} - \log M_{*,2}$ (lower panels) in halos of different mass ranges, as indicated. Similar to Fig. 7, results are shown for both case 1 (unshaded histograms) and case 2 (shaded histograms). In case 1, the isolated galaxies are put into the bin with $\log L_1 - \log L_2 = 2.0$ or $\log M_{*,1} - \log M_{*,2} = 2.0$.

TABLE 2
HALO OCCUPATION OF SATELLITE GALAXIES

Satellite galaxies	$\log M_{s,0}$	γ
(1)	(2)	(3)
< -18.0	12.48 ± 0.04	1.01 ± 0.06
-18.5	12.62 ± 0.02	1.05 ± 0.04
-19.0	12.77 ± 0.02	1.06 ± 0.03
-19.5	12.93 ± 0.01	1.07 ± 0.02
-20.0	13.15 ± 0.01	1.09 ± 0.02
-20.5	13.44 ± 0.01	1.10 ± 0.02
-21.0	13.82 ± 0.01	1.13 ± 0.02
-21.5	14.34 ± 0.01	1.33 ± 0.07

NOTE. — Halo occupation model parameters for satellite galaxies in the SDSS DR4. Here the mean halo occupations of satellite galaxies are described by $\langle N_s \rangle = (M_h/M_{s,0})^\gamma$. Column (1): The absolute magnitude limit of the satellite galaxies. Columns (2-3): the best fit parameters $M_{s,0}$ and γ (averages with errors). The errors are estimated from the variances between Samples II and III, with halo masses M_L and M_S , and are much larger than the errors obtained from our 200 bootstrap samples.

However, since the groups in our SDSS DR4 catalogue are not X-ray selected, a detailed comparison with our results is not possible. In a recent paper, D’Onghia et al. (2005) used detailed hydrodynamical simulations to predict the fraction of halos with $M_h \sim 10^{14} h^{-1} M_\odot$ that have $\log L_1 - \log L_2 \geq 0.8$. From a total of twelve simulated groups, they obtain a fossil fraction of 33 ± 16 percent. This value is much higher than the fraction of fossil systems we find in the SDSS, which suggests a potential over-merging problem in their simulations. More recently von Benda-Beckmann et al. (2007) used a combination of N-body simulations and empirical models for the connection between galaxy luminosity and halo mass (taken from Cooray & Milosavljević 2005), and found that the fossil group fraction is about 24% among all systems with masses $1 - 5 \times 10^{13.0} h^{-1} M_\odot$. This is in good agreement with our direct measurement from the SDSS data.

5. HALO-OCCUPATION STATISTICS

The upper panels of Fig. 9 show the mean halo occupation numbers, $\langle N \rangle$ (the mean number of all group members) and $\langle N_s \rangle$ (the mean number of satellites), as functions of halo mass M_h . Results are shown only for $M_h = M_L$, but adopting $M_h = M_S$ gives very similar results. The results shown in the left, middle and right panels correspond to galaxies in different luminosity ranges, as indicated in the panels. Similar to what is found in Y05c, the sharp break at the low mass end at $\langle N \rangle \sim 1$ ⁷ indicates an almost deterministic relation between the luminosity of a central galaxy and the mass of its dark matter halo. The shoulder suggests that the brightest satellite galaxies is in general much fainter than the central galaxy (e.g. Zheng et al. 2005). The mean number of satellite galaxies, which is shown as the dashed line, reveals a very good power law feature. To quantify this, we model the halo occupation for satellite galaxies with

$\langle N_s \rangle = (M_h/M_{s,0})^\gamma$, where $M_{s,0}$ is a characteristic halo mass above which there is on average at least one satellite galaxies and γ is the power law index. The best fit parameters for satellite galaxies with different absolute magnitude cuts are listed in Table 2. As an illustration, we show in the upper panels of Fig. 9 the corresponding best fit model predictions of the halo occupation of satellite galaxies as the dotted lines. They all agree with the data extremely well.

In addition to the mean halo occupation number, we also investigate the second moment of the halo occupation distribution (see Y05c). Here we only consider satellite galaxies, because by definition a central galaxy is always assigned to a group in a deterministic way. This quantity is crucial in modelling the two-point correlation function of galaxies on small scales (e.g., Benson et al. 2000; Berlind et al. 2003; Y05c; Tinker et al. 2007), and holds important information regarding the physical processes related to galaxy formation. In earlier investigations, a number of simple models were adopted to describe the second moment of the halo occupation distribution and its dependence on halo mass (e.g., Berlind & Weinberg 2002; Yang et al. 2003). In particular, using the group samples constructed from the 2dFGRS, Y05c measured the second moment for *all* group members and found that the halo occupation distribution is close to Poissonian in massive halos and significantly sub-Poissonian in low mass halos. In the middle row of Fig. 9, we show $\langle N_s^2 \rangle$ for *satellite* galaxies as a function of halo mass M_h . As one can see, $\langle N_s^2 \rangle$ is roughly proportional to M_h^2 . To see how the distribution deviates from a Poisson distribution, we show, in the lower panels of Fig 9, $\langle N_s^2 \rangle - \langle N_s \rangle^2$ as a function of $\langle N_s \rangle$. A Poisson distribution has $\langle N_s^2 \rangle - \langle N_s \rangle^2 = \langle N_s \rangle$ (dotted lines), while a deterministic distribution has $\langle N_s^2 \rangle - \langle N_s \rangle^2 \sim 0$. The results thus indicate that the number distribution of satellite galaxies follows roughly a Poisson distribution.

Fig. 10 shows the distribution of the number of satellite galaxies in groups, N_s , for different halo mass bins. The thick solid curves indicate Poisson distributions with the same $\langle N_s \rangle$. As one can see, the observed N_s -distributions are well fitted by Poisson distributions. These properties, which have already been found in Y05c, suggest a direct link between satellite galaxies and dark matter sub-halos. In a recent study, Kravtsov et al. (2004), using large numerical simulations, have shown that the occupation distribution of dark matter sub-halos follows Poisson statistics. This suggests that there may be a tight link between satellite galaxies and dark matter sub-halos, which has been a standard assumption in various HOD/CLF models (e.g., Vale & Ostriker 2004; 2006). Our results provide observational support for such a link.

6. SATELLITE FRACTIONS

The satellite fraction as function of luminosity, $f_{\text{sat}}(L)$, is an important quantity for a proper interpretation of measurements of galaxy-galaxy lensing (e.g., Guzik & Seljak 2002; Mandelbaum et al. 2006; Yang et al. 2006) and pairwise velocity dispersion of galaxies (e.g., Jing & Börner 2004; Slosar, Seljak & Tasitsiomi 2006; van den Bosch et al. 2007a; Li et al. 2007). In addition, since the halo bias depends on halo mass (Mo & White 1996), and since a satellite galaxy resides in a more massive halo

⁷ This is not seen in the upper left panel because our group catalogue does not include halos with masses below $10^{11.6} h^{-1} M_\odot$.

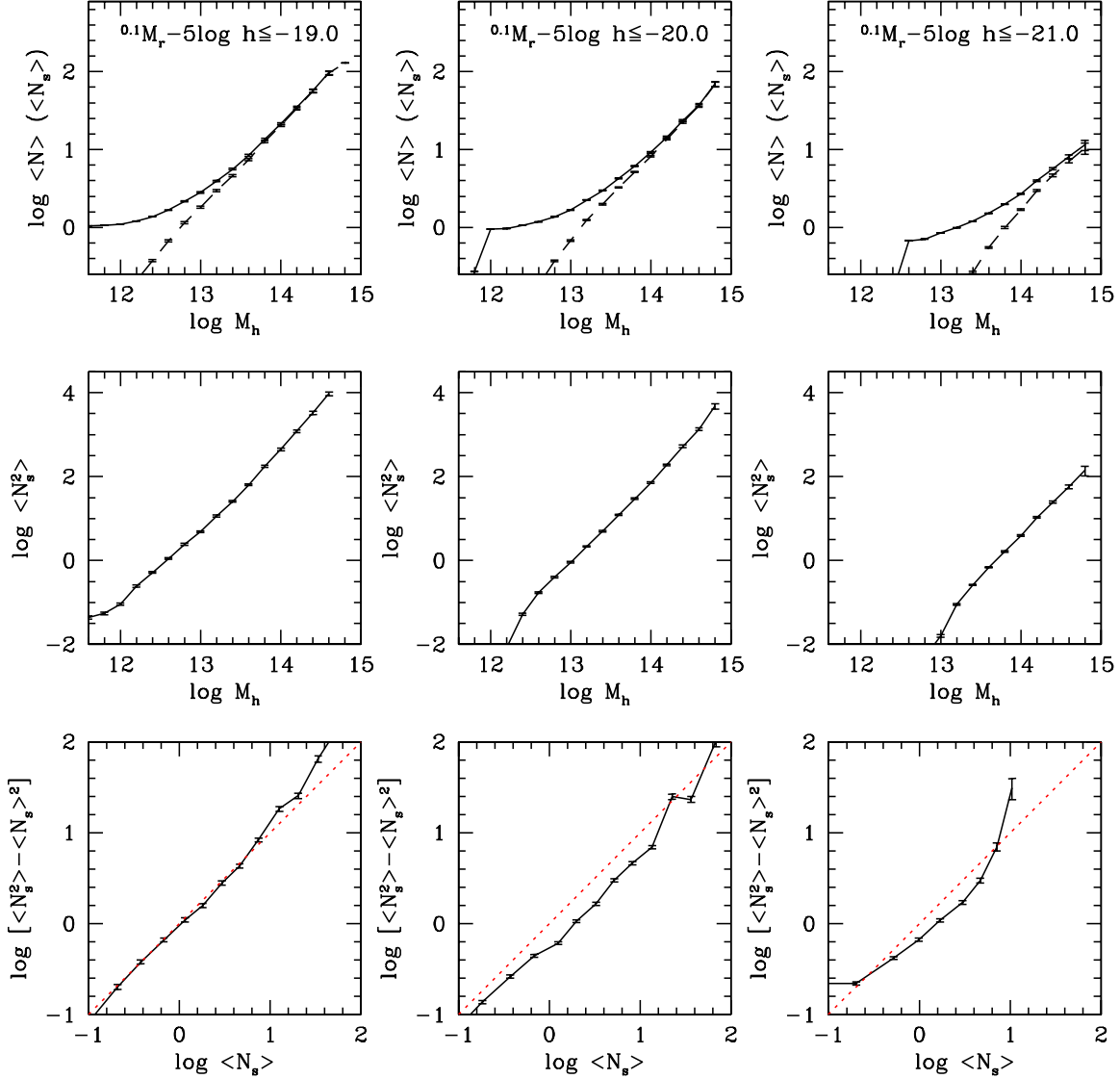


FIG. 9.— *Upper row of panels:* the average halo occupation numbers as function of halo mass for all galaxies ($\langle N \rangle$, solid lines) and for satellite galaxies only ($\langle N_s \rangle$, dashed lines). Here halo masses are taken to be M_L . Panels on the left, in the middle and on the right correspond to an absolute magnitude limit of $^{0.1}M_r - 5 \log h \leq -19.0$, -20.0 and -21.0 , respectively. The error-bars indicate the $1\text{-}\sigma$ variances obtained from 200 bootstrap samples. *Middle row of panels:* similar to the upper row of panels, except that here we plot the second moment of the occupation numbers of satellite galaxies, $\langle N_s^2 \rangle$. *Lower row of panels:* similar to the middle row of panels, except that now we plot $\langle N_s^2 \rangle - \langle N_s \rangle^2$ as function of $\langle N_s \rangle$. The dotted, diagonal line indicates $\langle N_s^2 \rangle - \langle N_s \rangle^2 = \langle N_s \rangle$ and corresponds to Poisson statistics. Apparently, the distribution of N_s is very similar to a Poisson distribution.

than a central galaxy of the same luminosity (van den Bosch et al. 2007b), the large scale clustering of galaxies of a given luminosity also depends strongly on the fraction of satellite galaxies. Here we estimate $f_{\text{sat}}(L)$ directly from our group catalogue. According to the test we carried out in the previous section, this fraction can be determined relatively accurately.

In the left-hand panel of Fig. 11 we show $f_{\text{sat}}(L)$ as a function of galaxy luminosity. The results are plotted separately for all (solid lines), red (dashed lines) and blue (dotted lines) galaxies. Since fiber collisions are expected to significantly impact the number of close pairs, it can affect the satellite fractions $f_{\text{sat}}(L)$. To assess the uncertainty induced by the fiber collisions, we show results for both Samples II and III, as thick and thin lines, respectively. As mentioned earlier, Samples II and III

may respectively under- and over-estimate the number of group members because of their different treatments of fiber collisions. Most likely the satellite fractions of these two extreme cases bracket the true satellite fractions. As one can see, the satellite fraction decreases with increasing luminosity, from $\sim 40\%$ at $^{0.1}M_r - 5 \log h = -17.0$ to $\sim 5\%$ at $^{0.1}M_r - 5 \log h = -22$. The satellite fraction of red galaxies at the faint end, $\sim 70\%$ at $^{0.1}M_r - 5 \log h = -17.0$, is significantly higher than that of blue galaxies, $\sim 30\%$ at $^{0.1}M_r - 5 \log h = -17.0$. The satellite fraction as a function of galaxy stellar mass is shown in the right panel of Fig. 11. The overall behavior here is similar to that shown in the left panel. For reference, we list in Table 3 the fraction of satellites as a function of galaxy luminosity or stellar mass, separately for all, red and blue galaxies. The averages listed in this

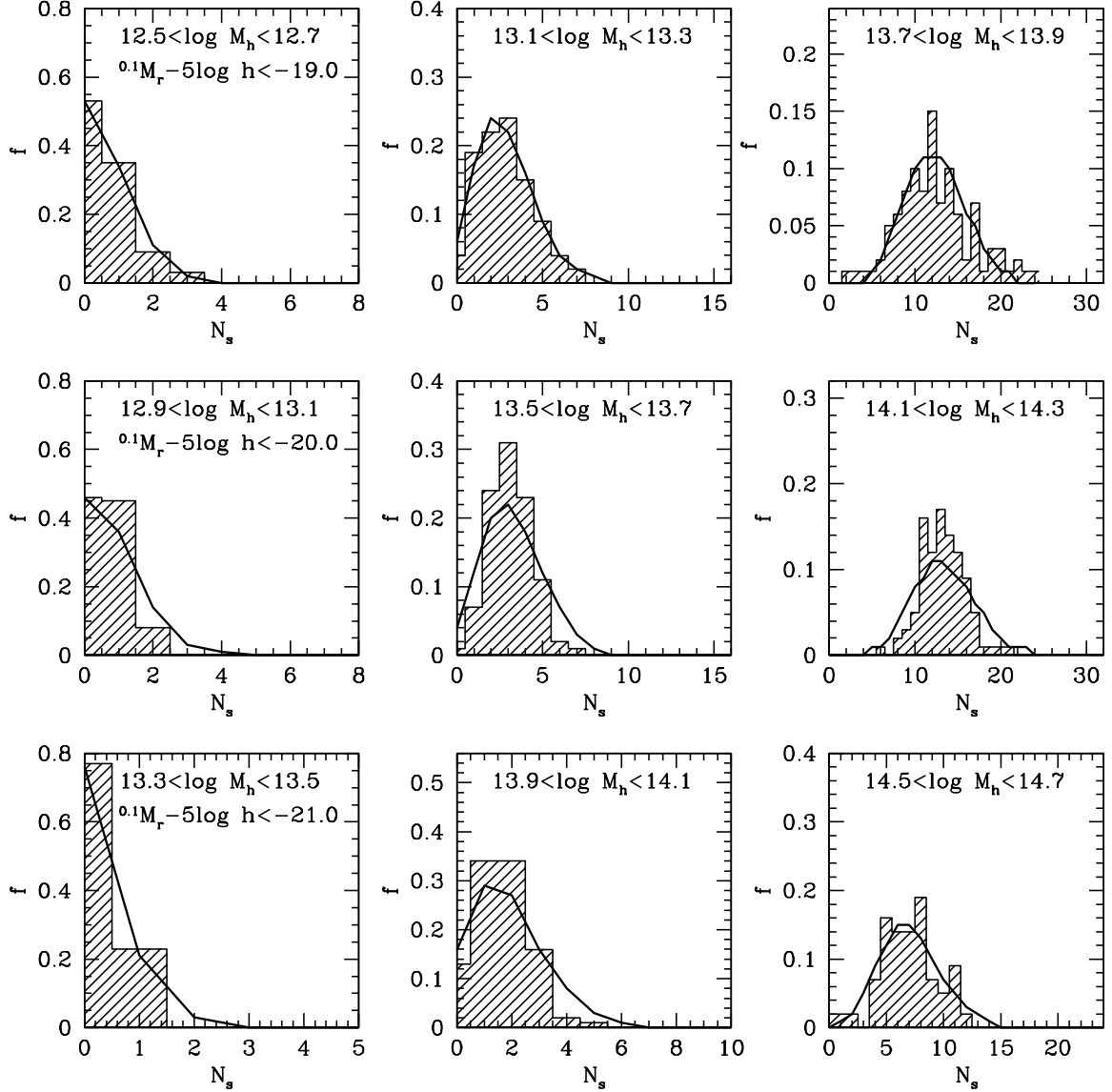


FIG. 10.— Number distributions of the satellite galaxies in groups of different halo mass bins, as indicated. Panels in the upper, middle and lower rows correspond to different absolute magnitude limits as indicated. The hatched histograms indicate the distributions obtained from the groups in the SDSS. Thick solid curves correspond to Poisson distributions with the same mean N_s , and are shown to illustrate the Poissonian nature of $P(N_s|M_h)$.

table are the averages between Sample II and III, while the errors quoted represent the deviations of the samples from the average.

In recent years, the fraction of satellite galaxies has been studied extensively using HOD/CLF models (Cooray 2006; Tinker et al. 2007; van den Bosch et al. 2007a), and analyses of galaxy-galaxy lensing measurements (e.g. Mandelbaum et al. 2006). For comparison, we overplot in Fig. 11 the results obtained by Mandelbaum et al. for early-type galaxies (solid circles) and late-type galaxies (open triangles), with error-bars indicating the 95% confidence level. Although their samples are defined differently from ours (they separate galaxies into early- and late-types according to galaxy morphologies, while we separate galaxies according to colour), our results match theirs quite well.

7. SUMMARY

Using a large galaxy group catalogue constructed from the SDSS Data Release 4 (DR4) by Y07, we have investigated various halo occupation statistics of galaxies. In particular, we have split the galaxy population in red and blue galaxies, and in centrals and satellites, and determined the conditional luminosity functions of these various subsamples. We have also presented luminosity gap statistics, satellite fractions, and halo occupation numbers for the galaxies in our group sample. The main results are summarized as follows:

1. The conditional luminosity functions for central and satellite galaxies can be well modelled with a log-normal distribution and a modified Schechter form, respectively. The corresponding best fitting parameters are listed in Table 1.
2. The average scatter of the log-normal luminosity distribution of central galaxies decreases from

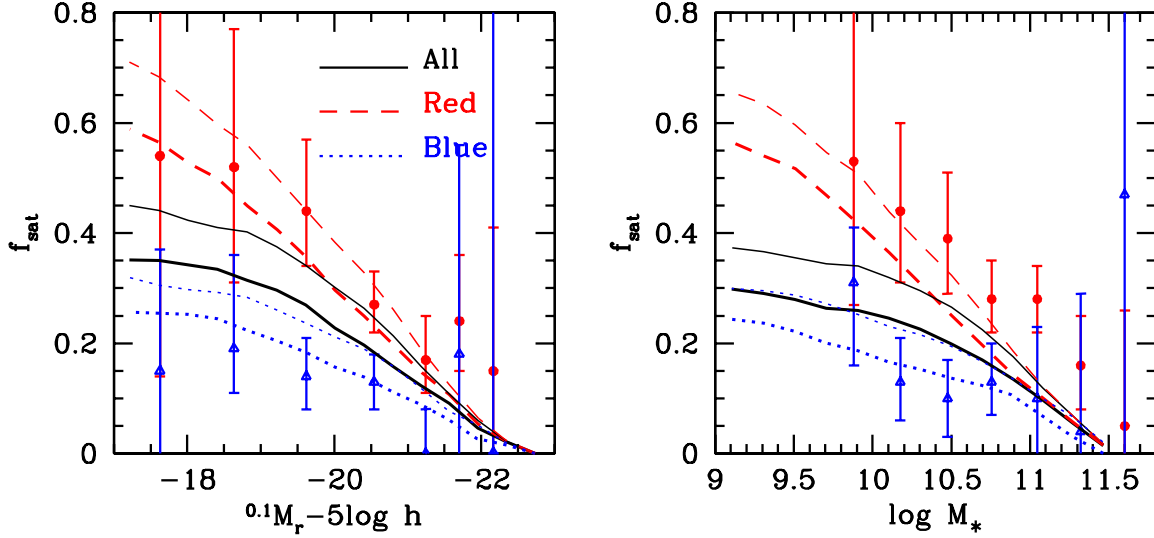


FIG. 11.— The fraction of satellite galaxies as function of luminosity (left-hand panel) and stellar mass (right-hand panel). Results are shown separately for all, red and blue galaxies as indicated. The thick lines are results for group Sample II and thin lines for group Sample III. For comparison, we show the satellite fractions obtained by Mandelbaum et al. (2006) from a galaxy-galaxy lensing analysis of the SDSS as the solid circles and open triangles with vertical errorbars (95% CL) for early- and late-type galaxies, respectively

TABLE 3
SATELLITE FRACTIONS

Galaxy	All	Red	Blue
(1)	(2)	(3)	(4)
-22.34	0.021 ± 0.001	0.023 ± 0.001	0.017 ± 0.003
-21.95	0.053 ± 0.010	0.058 ± 0.008	0.040 ± 0.018
-21.56	0.100 ± 0.012	0.116 ± 0.013	0.069 ± 0.011
-21.18	0.141 ± 0.025	0.167 ± 0.029	0.104 ± 0.021
-20.80	0.186 ± 0.040	0.230 ± 0.045	0.135 ± 0.033
-20.41	0.230 ± 0.047	0.289 ± 0.055	0.164 ± 0.036
-20.01	0.264 ± 0.052	0.340 ± 0.062	0.185 ± 0.039
-19.61	0.306 ± 0.050	0.400 ± 0.060	0.211 ± 0.037
-19.22	0.336 ± 0.056	0.453 ± 0.067	0.233 ± 0.040
-18.82	0.358 ± 0.062	0.505 ± 0.078	0.253 ± 0.042
-18.41	0.372 ± 0.054	0.548 ± 0.069	0.269 ± 0.033
-18.01	0.382 ± 0.057	0.584 ± 0.080	0.275 ± 0.031
-17.61	0.396 ± 0.064	0.624 ± 0.083	0.280 ± 0.035
-17.21	0.400 ± 0.070	0.650 ± 0.086	0.288 ± 0.044
11.28	0.061 ± 0.009	0.062 ± 0.008	0.049 ± 0.026
11.08	0.108 ± 0.016	0.112 ± 0.015	0.084 ± 0.022
10.89	0.155 ± 0.029	0.164 ± 0.030	0.123 ± 0.022
10.70	0.197 ± 0.039	0.226 ± 0.042	0.146 ± 0.031
10.50	0.233 ± 0.047	0.287 ± 0.051	0.166 ± 0.041
10.30	0.260 ± 0.049	0.343 ± 0.051	0.185 ± 0.045
10.10	0.282 ± 0.052	0.401 ± 0.052	0.199 ± 0.046
9.91	0.300 ± 0.057	0.461 ± 0.064	0.220 ± 0.047
9.70	0.304 ± 0.057	0.507 ± 0.055	0.237 ± 0.050
9.51	0.317 ± 0.054	0.557 ± 0.057	0.255 ± 0.046
9.31	0.328 ± 0.054	0.587 ± 0.066	0.266 ± 0.041
9.11	0.336 ± 0.053	0.610 ± 0.064	0.271 ± 0.039

NOTE. — Satellite fractions of galaxies in the SDSS DR4, as function of galaxy luminosity and stellar mass. Results are listed for all, red and blue galaxies, respectively. Column (1): The average luminosity ($^{0.1}M_r - 5 \log h$; upper part) and stellar mass ($\log[M_*/h^{-2} M_\odot]$; lower part) of galaxies. Columns (2-4): the fractions of satellite galaxies for all, red and blue galaxies (averages with errors). The errors are estimated from the variances between Samples II and III, and are much larger than the errors obtained from our 200 bootstrap samples.

~ 0.15 dex at the massive end ($\log[M_h/h^{-1}M_\odot] \gtrsim 13.5$) to ~ 0.1 dex at the low mass end ($\log[M_h/h^{-1}M_\odot] \sim 12.0$). However, due to the method used to assign halo masses to the groups, at the low mass end this should be considered a lower limit on the true amount of scatter.

3. The slope of the relation between the average luminosity of central galaxies (in the $^{0.1}r$ -band) and halo mass, $d \log L_c / d \log M_h$, decreases from ~ 0.68 for $\log[M_h/h^{-1}M_\odot] \ll 12.5$ to ~ 0.17 for $\log[M_h/h^{-1}M_\odot] \gg 12.5$. For the stellar masses of the central galaxies we obtain that $d \log M_{*,c} / d \log M_h$, decreases from ~ 1.83 for $\log[M_h/h^{-1}M_\odot] \ll 12.1$ to ~ 0.22 for $\log[M_h/h^{-1}M_\odot] \gg 12.1$.
4. The halo (group) occupation numbers of satellite galaxies accurately follow Poisson statistics. Since the same applies to dark matter sub-halos, this supports the standard picture that satellite galaxies are associated with dark matter sub-halos.
5. In massive halos with masses $M_h \gtrsim 10^{14} h^{-1}M_\odot$ roughly 85% (80%) of the central (satellite) galaxies are red. These red fractions decrease to 50% (40%) in halos with masses $M_h \sim 10^{12} h^{-1}M_\odot$.
6. By comparing the scatter in the luminosities of BCGs to the luminosity difference between the BCG and its brightest satellite, we find that the BCGs form a ‘special’ subclass, in that their luminosities can not be considered the extreme values of the distribution of satellite luminosities, especially in halos with masses $M_h \lesssim 10^{14.0} h^{-1}M_\odot$.
7. The fractions of fossil groups, which are defined as groups with luminosity gap $\log L_1 - \log L_2 \geq 0.8$, decreases with increasing of halo mass from 18%-60% in halos with $M_h \sim 10^{13} h^{-1}M_\odot$ to $\sim 2.5\%$ in halos with $M_h \sim 10^{14} h^{-1}M_\odot$.

8. The satellite fractions obtained from our group catalogue as functions of both luminosity and stellar mass (listed in Table 3) are in good agreement with independent constraints from analyses of galaxy clustering and galaxy-galaxy lensing.

These results can be used to constrain the various physical processes related to galaxy formation and to interpret the various statistics used to describe large scale structures (e.g., galaxy correlation functions, pairwise velocity dispersions, etc.). Most of our findings are in good agreement with previous studies (e.g. Y05c, Zandivarez et al. 2006; Robotham et al. 2006) and can be linked to the semi-analytical modelling of galaxy formations (e.g., Kang et al. 2005; Zheng et al. 2005; Bower et al. 2006; Croton et al. 2006; De Lucia et al. 2007). The luminosity and stellar mass gap can be used to probe the specific formation properties of central galaxies (e.g., Vale & Ostriker 2007). The fraction of the red and blue populations for central and satellite galaxies can be used to probe the color evolution of satellite galaxies (van den Bosch et al. 2007b).

ACKNOWLEDGMENTS

We thank J.P. Ostriker and Zheng Zheng for helpful comments, and Cheng Li for the galaxy color bi-normal fitting. XY is supported by the *One Hundred Talents* project, Shanghai Pujiang Program (No. 07pj14102), 973 Program (No. 2007CB815402), the CAS Knowledge

Innovation Program (Grant No. KJCX2-YW-T05) and grants from NSFC (Nos. 10533030, 10673023). HJM would like to acknowledge the support of NSF AST-0607535, NASA AISR-126270 and NSF IIS-0611948. Funding for the SDSS and SDSS-II has been provided by the Alfred P. Sloan Foundation, the Participating Institutions, the National Science Foundation, the U.S. Department of Energy, the National Aeronautics and Space Administration, the Japanese Monbukagakusho, the Max Planck Society, and the Higher Education Funding Council for England. The SDSS Web Site is <http://www.sdss.org/>. The SDSS is managed by the Astrophysical Research Consortium for the Participating Institutions. The Participating Institutions are the American Museum of Natural History, Astrophysical Institute Potsdam, University of Basel, Cambridge University, Case Western Reserve University, University of Chicago, Drexel University, Fermilab, the Institute for Advanced Study, the Japan Participation Group, Johns Hopkins University, the Joint Institute for Nuclear Astrophysics, the Kavli Institute for Particle Astrophysics and Cosmology, the Korean Scientist Group, the Chinese Academy of Sciences (LAMOST), Los Alamos National Laboratory, the Max-Planck-Institute for Astronomy (MPIA), the Max-Planck-Institute for Astrophysics (MPA), New Mexico State University, Ohio State University, University of Pittsburgh, University of Portsmouth, Princeton University, the United States Naval Observatory, and the University of Washington.

REFERENCES

- Adelman-McCarthy J.K., et al., 2006, *ApJS*, 162, 38
 Baldry I.K., Glazebrook K., Brinkmann J., Ivezić Z., Lupton R.H., Nichol R.C., Szalay A.S., 2004, *ApJ*, 600, 681
 Baldry I.K., Balogh M.L., Bower R.G., Glazebrook K., Nichol R.C., Bamford S.P., Budavari T., 2006, *MNRAS*, 373, 469
 Bell E.F., McIntosh D.H., Katz N., Weinberg M.D., 2003, *ApJS*, 149, 289
 Benson A.J., Cole S., Frenk C.S., Baugh C.M., Lacey C.G., 2000, *MNRAS*, 311, 793
 Berlind A.A., Weinberg D.H., 2002, *ApJ*, 575, 587
 Berlind A.A., Weinberg D.H., Benson A.J., Baugh C.M., Cole S., Dave R., Frenk C.S., Jenkins A., Katz N., Lacey C.G., 2003, *ApJ*, 593, 1
 Berlind A.A., et al. 2006, *ApJS*, 167, 1
 Berlind A.A., Kazin E., Blanton M.R., Pueblas S., Scoccimarro R., Hogg D.H., 2007, preprint (astro-ph/0610524)
 Blanton M. R. et al. , 2003a, *ApJ*, 592, 819
 Blanton M. R. et al. , 2003b, *AJ*, 125, 2348
 Blanton M.R., Eisenstein D.J., Hogg D.W., Schlegel D.J., Brinkmann J., 2005a, *ApJ*, 629, 143
 Blanton M.R. et al. , 2005b, *AJ*, 129, 2562
 Bower R.G., Benson A.J., Malbon R., Helly J.C., Frenk C.S., Baugh C.M., Cole S., Lacey C.G., 2006, *MNRAS*, 370, 645
 Bullock J.S., Wechsler, R.H., Somerville R.S., 2002, *MNRAS*, 329, 246
 Coil A.L., et al., 2006, *ApJ*, 638, 668
 Collister A.A., Lahav O., 2005, *MNRAS*, 361, 415
 Cooray A., 2005, *MNRAS*, 364, 303
 Cooray A., 2006, *MNRAS*, 365, 842
 Cooray A., Milosavljević M., 2005, *ApJ*, 627, L89
 Croton D.J., et al. 2006, *MNRAS*, 365, 11
 Dekel A., 2004, preprint (astro-ph/0401503)
 De Lucia G., et al. 2007, *MNRAS*, 374, 809
 D’Onghia E., Sommer-Larsen J., Romeo A.D., Burkert A., Pedersen K., Portinari L., Rasmussen J., 2005, *ApJ*, 630, L109
 Guzik J., Seljak U., 2002, *MNRAS*, 335, 311
 Hansen S.M., Sheldon E.S., Wechsler R.H., Koester B.P., 2007, preprint (arXiv:0710.3780)
 Jing Y.P., Mo H.J., Börner G., 1998, *ApJ*, 494, 1
 Jing Y.P., Börner G., Suto Y., 2002, *ApJ*, 564, 15
 Jing Y.P., Börner G., 2004, *ApJ*, 617, 782
 Jones L.R., Ponman T.J., Horton A., Babul A., Ebeling H., Burke D.J., 2003, *MNRAS*, 343, 627
 Kang X., Jing Y.P., Mo H.J., Börner G., 2002, *MNRAS*, 336, 892
 Kang X., Jing Y.P., Mo H.J., Börner G., 2005, *ApJ*, 631, 21
 Kauffmann G., White S.D.M., Guiderdoni B., 1993, *MNRAS*, 264, 201
 Kravtsov A.V., Berlind A.A., Wechsler R.H., Klypin A.A., Gottlöber S., Allgood B., Primack J.R., 2004, *ApJ*, 609, 35
 Li C., Kauffmann G., Jing Y.P., White S.D.M., Börner G., Cheng F.Z., 2006, *MNRAS*, 368, 21
 Li C., Jing Y.P., Kauffmann G., Börner G., Kang X., Wang L., 2007, *MNRAS*, 376, 984
 Lin Y.T., Mohr J.J., 2004, *ApJ*, 617, 879
 McIntosh D.H., Guo Y., Hertzberg J., Katz N., Mo H.J., van den Bosch F.C., Yang X., 2007, preprint (arXiv:0710.2157)
 Magliocchetti M., Porciani C., 2003, *MNRAS*, 346, 186
 Mandelbaum R., Seljak U., Kauffmann G., Hirata C.M., Brinkmann J., 2006, *MNRAS*, 368, 715
 Marinoni C., Hudson M.J., 2002, *ApJ*, 569, 101
 Milosavljević M., Miller C.J., Furlanetto S.R., Cooray A., 2006, *ApJ*, 637, L9
 Mo H.J., White S.D.M., 1996, *MNRAS*, 282, 347
 Mo H.J., Yang X.H., van den Bosch F.C., Jing Y.P., 2004, *MNRAS*, 349, 205
 Peacock J.A., Smith R.E., 2000, *MNRAS*, 318, 1144
 Petrosian V., 1976, *ApJ*, 209, L1
 Robotham A., Wallace C., Philipps S., De Propriis R., 2006, *ApJ*, 652, 1077
 Sales L.V., Navarro J.F., Lambas D.G., White S.D.M., Croton D.J., 2007, preprint (arXiv:0706.2009)
 Schlegel D.J., Finkbeiner D.P., Davis M., 1998, *ApJ*, 500, 525
 Scoccimarro R., Sheth R.K., Hui L., Jain B., 2001, *ApJ*, 546, 20
 Scranton R., 2002a, *MNRAS*, 332, 697
 Seljak U., 2000, *MNRAS*, 318, 203
 Slosar A., Seljak U., Tasitsiomi A., 2006, *MNRAS*, 366, 1455
 Sommer-Larsen J., 2006, *MNRAS*, 369, 958
 Strauss M.A., et al., 2002, *AJ*, 124, 1810
 Tinker J.L., Weinberg D.H., Zheng Z., Zehavi I., 2005, *ApJ*, 631, 41
 Tinker J.L., Norberg P., Weinberg D.H., Warren M.S., 2007, *ApJ*, 659, 877
 Tremaine S.D., Richstone D.O., 1977, *ApJ*, 212, 311
 Vale A., Ostriker J.P., 2004, *MNRAS*, 353, 189
 Vale A., Ostriker J.P., 2006, *MNRAS*, 371, 1173
 Vale A., Ostriker J.P., 2007, preprint (astro-ph/0701096)
 van den Bosch F.C., Yang X., Mo H.J., 2003, *MNRAS*, 340, 771
 van den Bosch F.C., Mo H.J., Yang X., 2003, *MNRAS*, 345, 923

- van den Bosch F.C., Weinmann S.M., Yang X., Mo H.J., Li C., Jing Y.P., 2005, MNRAS, 361, 1203
- van den Bosch F.C., Yang X., Mo H.J., Weinmann S.M., Maccio A., More S., Cacciato M., Skibba R., Kang X., 2007a, MNRAS, 376, 841
- van den Bosch F.C., Aquino D., Yang X., Mo H.J., Pasquali A., McIntosh D.H., Weinmann S.M., Kang X., 2007b, preprint (arXiv:0710.3164)
- Vikhlin A., McNamara B.R., Hornstrup A., Quintana H., Forman W., Jones, C., Way C., 1999, ApJ, 520, L1
- von Benda-Beckmann A.M., D’Onghia E., Gottloeber S., Hoeft M., Khalatyan A., Klypin A., Mueller V., 2007, preprint (arXiv:0710.1297)
- Weinmann S.M., van den Bosch F.C., Yang X., Mo H.J., 2006a, MNRAS, 366, 2
- Weinmann S.M., van den Bosch F.C., Yang X., Mo H.J., Croton D.J., Moore, B., 2006b, MNRAS, 372, 1161
- Wang Y., Yang X.H., Mo H.J., van den Bosch F.C., Chu Y., 2004, MNRAS, 353, 287
- White M., Zheng Z., Brown M.J.I., Dey A., Jannuzi B.T., 2007, ApJ, 655, 69
- Yan R., Madgwick D.S., White M., 2003, ApJ, 598, 848
- Yan R., White M., Coil A.L., 2004, ApJ, 607, 739
- Yang X., Mo H.J., van den Bosch F.C., 2003, MNRAS, 339, 1057
- Yang X., Mo H.J., Jing Y.P., van den Bosch F.C., Chu Y.Q., 2004, MNRAS, 350, 1153
- Yang X., Mo H.J., van den Bosch F.C., Jing Y.P., 2005a, MNRAS, 356, 1293
- Yang X., Mo H.J., van den Bosch F.C., Jing Y.P., 2005b, MNRAS, 357, 608
- Yang X., Mo H.J., Jing Y.P., van den Bosch F.C. 2005c, MNRAS, 358, 217 (Y05c)
- Yang X., Mo H.J., van den Bosch F.C., Weinmann S.M., Li C., Jing Y.P., 2005d, MNRAS, 362, 711
- Yang X., Mo H.J., van den Bosch F.C., 2006, ApJ, 638L, 55
- Yang X., Mo H.J., van den Bosch F.C., Pasquali A., Li C., Barden M., 2007, ApJ, 671, 153 (paper 1, Y07)
- Zandivarez A., Martinez H.J., Merchán M.E., 2006, ApJ, 650, 137
- Zehavi I., et al., 2002, ApJ, 571, 172
- Zehavi I., et al., 2004 ApJ, 608, 16
- Zehavi I., et al., 2005 ApJ, 630, 1
- Zheng Z., Tinker J.L., Weinberg D.H., Berlind A.A., 2002, ApJ, 575, 617
- Zheng Z., et al., 2005, ApJ, 633, 791
- Zheng Z., Coil A.L., Zehavi I., 2007, ApJ, 667, 760
- Zheng Z., Weinberg D.H., 2007, ApJ, 659, 1